Effects of Metal Ions on the Electronic, Redox, and Catalytic Properties of Cofactor TTQ of Quinoprotein Amine Dehydrogenases

Shinobu Itoh,*,† Masato Taniguchi,‡ Naoki Takada,‡ Shigenori Nagatomo,§ Teizo Kitagawa,*,§ and Shunichi Fukuzumi*,‡

Contribution from the Department of Chemistry, Graduate School of Science, Osaka City University, 3-3-138 Sugimoto, Sumiyoshi-ku, Osaka 558-8585, Japan, Department of Material and Life Science, Graduate School of Engineering, Osaka University, CREST, Japan Science and Technology Corporation, 2-1 Yamada-oka, Suita, Osaka 565-0871, Japan, and Institute for Molecular Science, Myodaiji, Okazaki 444-8585, Japan

Received June 6, 2000

Abstract: Model compounds of novel organic cofactor TTQ (tryptophan tryptophylquinone) of quinoprotein methylamine and aromatic amine dehydrogenases have been shown to interact with a series of metal ions in anhydrous organic media. Spectroscopic analyses including UV−vis, NMR, and resonance Raman indicate that the metal ion binds to the TTQ model compounds at their *o*-quinone moiety, the binding mode of which is similar to that proposed for the interaction between cofactor TTQ and a cationic species in the native enzymes. The binding constants K_{ML} for the metal ion complexes of TTQ model compounds have been determined from the spectral changes in UV−vis due to the complex formation. Remarkable enhancement of the oxidizing ability of the TTQ model compounds by the complexation with metal ions has been demonstrated as a large positive shift in the one-electron reduction potentials E^0_{red} of the complexes as compared to those of the TTQ model compounds in metal free form (e.g. $\Delta E^0_{red} = 1.17$ V for the Mg^{2+} complex and $\Delta E^0_{red} = 1.16$ V for the Sc^{3+} complex). The complexes can oxidize not only benzylamine but also aliphatic amines in anhydrous acetonitrile, whereas no reaction takes place in the absence of the metal ion under otherwise the same experimental conditions. Kinetic studies have revealed that the reaction proceeds via a transamination mechanism involving iminoquinone and product imine intermediates to yield the oxidized products and the reduced TTQ. The ESR spectra of the half-reduced species of TTQ model compounds, i.e. semiquinone radical anions, are detected successfully. The spin distribution derived from the hyperfine structures indicates that the spin is partially delocalized on the indole ring connected at the 4-position of the quinone skeleton. This indicates that the indole group plays an important role as a part of the electron-transfer pathway from the reduced TTQ to a blue copper protein in biological systems.

Introduction

Bacterial methylamine dehydrogenase (MADH) and aromatic amine dehydrogenase (AADH) are new members of quinoprotein (quinone-containing enzymes), which involve a heterocyclic *o*-quinone cofactor TTQ (tryptophan tryptophylquinone) at their active sites of the light subunits.[1−3] This cofactor is posttranslationally derived from two tryptophan residues in the enzyme active site,[1,4] acting as the redox catalyst for the enzymatic oxidation of primary amines to the corresponding aldehydes (eq 1). Davidson and co-workers[5−7] have demonstrated that the

$$CH_3NH_2 + H_2O \xrightarrow{2e^-,\ 2H^+} HCHO + NH_3 \quad (1)$$

enzymatic amine-oxidation proceeds via a *transamination mechanism* shown in Scheme 1, which has been verified by model studies using a series of TTQ model compounds in nonenzymatic systems.[8−11] Two electrons, taken in the amine-oxidation reaction, are successively transferred to a blue copper

Scheme 1

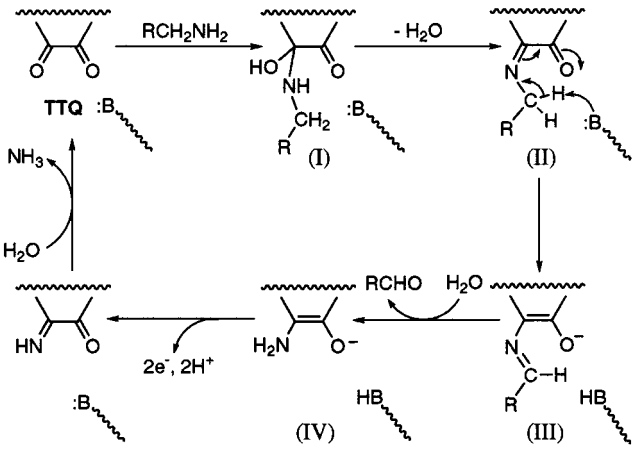

† Osaka City University.
‡ Osaka University.
§ Institute for Molecular Science.

(1) McIntire, W. S.; Wemmer, D. E.; Chistoserdov, A.; Lidstrom, M. E. *Science* **1991**, *252*, 817−824.
(2) Chen, L.; Mathews, F. S.; Davidson, V. L.; Huizinga, E. G.; Vellieux, F. M. D.; Hol, W. G. J. *Proteins* **1992**, *14*, 288−299.
(3) Govindaraj, S.; Eisenstein, E.; Jones, L. H.; Sanders-Loehr, J.; Chistoserdov, A. Y.; Davidson, V. L.; Edwards, S. L. *J. Bacteriol.* **1994**, *176*, 2922−2929.
(4) Chistoserdov, A. Y.; Tsygankov, Y. D.; Lidstrom, M. E. *Biochem. Biophys. Res. Commun.* **1990**, *172*, 211−216.

10.1021/ja0020207 CCC: $19.00
Published on Web 11/23/2000

protein such as amicyanin or azurin through an electron-transfer complex between the two enzymes: amine dehydrogenase and blue copper protein.[12,13] The crystal structure of the electron-transfer complex of the enzymes has suggested that the indole ring connected at the 4-position of the quinone ring of TTQ acts as a part of the electron-transfer pathway from the reduced quinone to the electron acceptor protein.[12]

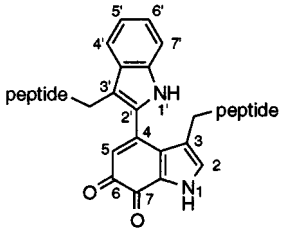

TTQ

Monovalent cations such as ammonium ion and alkaline metal ions have recently been shown to influence not only the UV−vis spectrum of the cofactor but also the reactivity of TTQ in the amine-oxidation reaction and in the electron transfer from the reduced TTQ to amicyanin.[14−19] It has been demonstrated that the enzymes have two different cation binding sites, one of which is located near the quinone carbonyl oxygen O(6) of the cofactor. The cationic species incorporated into this binding region have been suggested to interact directly with the quinone moiety, affecting the electronic structure of the cofactor as well as the reactivity in both the amine-oxidation reaction and the subsequent electron-transfer process. It has also been reported that the semiquinone radical of TTQ in the enzyme active site is largely stabilized by the interaction with the cationic species.[16] However, very little is known about the binding model of the cationic species toward TTQ or as to how they affect the redox properties of the cofactor. Thus, studies on interaction between TTQ model compounds and a series of metal ions and their catalytic effects on the redox properties of TTQ are required to provide an important clue to guide the search for the actual role of cationic species in the TTQ-dependent enzymatic functions.

This study reports for the first time that TTQ model compounds (**1**−**4**) can form complexes with a series of metal ions and that the metal ions can catalyze the amine oxidation by TTQ model compounds in nonenzymatic systems.[20] Remarkable enhancement of the oxidizing ability of the TTQ model compounds by complexation with metal ions is shown by the electrochemical studies. Although most of the metal ions employed in this study have no proven biological role at present, extensive studies on the effects of metal ions on the electronic structures and redox properties of TTQ model compounds reported herein provide profound insight into the actual role of the cationic species in the enzymatic functions. The ESR spectra of the half-reduced species of TTQ model compounds, i.e. semiquinone radical anions, are also reported in this study. The spin distribution derived from the hyperfine structures of the ESR spectra implicates an important role of the indole ring at the 4-position as an electron-transfer pathway from the reduced TTQ to a blue copper protein in the biological systems. Furthermore, interaction between metal ions and redox coenzymes has long been one of the most attractive subjects in electron-transfer chemistry.[21] Thus, the present study will add a new area of metal ion catalysis on the redox functions of *o*-quinone cofactors.

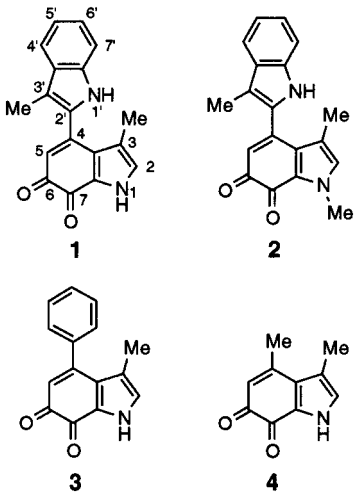

Experimental Section

Materials. The TTQ model compounds (**1**−**4**) were obtained from previous studies.[8−10] All other chemicals used in this study were commercial products of the highest available purity and were further purified by the standard methods, if necessary.[22]

Titration. The binding constants (K_{ML}) for the 1:1 complex formation between the quinones (5.0×10^{-5} M) and metal ions (M^{n+}, $n = 1-3$)

(5) Davidson, V. L.; Jones, L. H.; Graichen, M. E. *Biochemistry* **1992**, *31*, 3385−3390.
(6) Warncke, K.; Brooks, H. B.; Babcock, G. T.; Davidson, V. L.; McCracken, J. *J. Am. Chem. Soc.* **1993**, *115*, 6464−6465.
(7) Hyun, Y.-L.; Davidson, V. L. *Biochemistry* **1995**, *34*, 816−823.
(8) Itoh, S.; Ogino, M.; Haranou, S.; Terasaka, T.; Ando, T.; Komatsu, M.; Ohshiro, Y.; Fukuzumi, S.; Kano, K.; Takagi, K.; Ikeda, T. *J. Am. Chem. Soc.* **1995**, *117*, 1485−1493.
(9) Itoh, S.; Takada, N.; Haranou, S.; Ando, T.; Komatsu, M.; Ohshiro, Y.; Fukuzumi, S. *J. Org. Chem.* **1996**, *61*, 8967−8974.
(10) Itoh, S.; Takada, N.; Ando, T.; Haranou, S.; Huang, X.; Uenoyama, Y.; Ohshiro, Y.; Komatsu, M.; Fukuzumi, S. *J. Org. Chem.* **1997**, *62*, 5898−5907.
(11) Kano, K.; Nakagawa, M.; Takagi, K.; Ikeda, T. *J. Chem. Soc., Perkin Trans. 2* **1997**, 1111−1119.
(12) Chen, L.; Durley, R.; Poliks, B. J.; Hamada, K.; Chen, Z.; Mathews, F. S.; Davidson, V. L.; Satow, Y.; Huizinga, E.; Vellieux, F. M. D.; Hol, W. G. J. *Biochemistry* **1992**, *31*, 4959−4964.
(13) (a) Chen, L.; Durley, R. C. E.; Mathews, F. S.; Davidson, V. L. *Science* **1994**, *264*, 86−90. (b) Chen, L.; Mathews, F. S.; Davidson, V. L.; Tegoni, M.; Rivetti, C.; Rossi, G. L. *Protein Sci.* **1993**, *2*, 147−154. (c) Brooks, H. B.; Davidson, V. L. *Biochemistry* **1994**, *33*, 5696−5701. (d) Brooks, H. B.; Davidson, V. L. *J. Am. Chem. Soc.* **1994**, *116*, 11201−11202. (e) Bishop, G. R.; Davidson, V. L. *Biochemistry* **1995**, *34*, 12082−12086. (f) Hyun, Y.-L.; Davidson, V. L. *Biochemistry* **1995**, *34*, 12249−12254. (g) Davidson, V. L.; Jones, L. H. *J. Biol. Chem.* **1995**, *270*, 23941−23943. (h) Davidson, V. L.; Jones, L. H. *Biochemistry* **1996**, *35*, 8120−8125. (i) Merli, A.; Brodersen, D. E.; Morini, B.; Chen, Z.; Durley, R. C. E.; Mathews, F. S.; Davidson, V. L.; Rossi, G. L. *J. Biol. Chem.* **1996**, *271*, 9177−9180. (j) Davidson, V. L.; Jones, L. H.; Graichen, M. E.; Mathews, F. S.; Hosler, J. P. *Biochemistry* **1997**, *36*, 12733−12738. (k) Davidson, V. L.; Jones, L. H.; Zhu, Z. *Biochemistry* **1998**, *37*, 7371−7377.
(14) Kuusk V.; McIntire, W. S. *J. Biol. Chem.* **1994**, *269*, 26136−26143.
(15) Gorren A. C. F.; Duine, J. A. *Biochemistry* **1994**, *33*, 12202−12209.
(16) Gorren, A. C. F.; de Vries, S.; Duine, J. A. *Biochemistry* **1995**, *34*, 9748−9754.
(17) Gorren, A. C. F.; Moenne-Loccoz, P.; Backes, G.; de Vries, S.; Sanders-Loehr, J.; Duine, J. A. *Biochemistry* **1995**, *34*, 12926−12931.
(18) Moenne-Loccoz, P.; Nakamura, N.; Itoh, S.; Fukuzumi, S.; Gorren, A. C. F.; Duine, J. A.; Sanders-Loehr, J. *Biochemistry* **1996**, *35*, 4713−4720.
(19) Bishop G. R.; Davidson, V. L. *Biochemistry* **1997**, *36*, 13586−13592.
(20) For preliminary results, see: Itoh, S.; Taniguchi, M.; Fukuzumi, S. *Chem. Commun.* **2000**, 329−330.
(21) (a) Fukuzumi, S. *Advances in Electron-Transfer Chemistry*; Mariano, P. S., Ed.; JAI Press: Greenwich, CT, 1992; Vol. 2, pp 67−175. (b) Fukuzumi, S. *Electron Transfer in Chemistry*; Balzani, V., Ed.; Wiley-VCH: Weinheim, 2000; Vol. 5, in press.
(22) Perrin, D. D.; Armarego, W. L. F. *Purification of Laboratory Chemicals*; Butterworth-Heinemann: Oxford, 1988.

were determined by spectrophotometric titration using a 1 cm path length UV cell in anhydrous CH_3CN. Details about the experimental conditions are cited in the figure captions, and the experimental results were summarized in Tables 1 and 3.

Visible Resonance Raman Measurement. Visible resonance Raman scattering was excited at 413.1 nm with a Kr^+ ion laser (Spectra Physics, Model 2060), dispersed with a 100 cm single polychlomator (Ritsu Oyo Kogaku, Model MC-100DG), and detected with a CCD detector (Princeton Instruments, Model LN/CCD-1340 × 400PB). Sample solutions were contained in a spinning cell (1000 rpm) and kept at 25 °C. The slit width and slit height were set to be 200 μm and 20 mm, respectively. The wavenumber width per a channel of detector, which determines the spectral resolution, was 0.33 cm^{-1}. Raman shifts were calibrated with indene as a standard and the accuracy of peak positions was ± 1 cm^{-1} for well-defined bands.

Kinetic Analysis. The reaction of **1** and an amine was followed by UV−vis spectra using a Hewlett-Packard 8453 photodiode array spectrophotometer under the pseudo-first-order conditions with excess amine in deaerated CH_3CN at 25 °C. Typically, a CH_3CN solution containing **1** (5.0×10^{-5} M) and a metal ion was placed in a UV cell (1 cm path length, sealed tightly with a silicon rubber cap) and deaerated by bubbling Ar through it for ca. 20 min. Then the amine was added with a microsyringe to start the reaction. The pseudo-first-order rate constant (k_{obs}) was determined from the rate of a decrease in the intensity of the absorption due to the quinone or an increase in the intensity of the absorption due to the intermediate or the reduced product of the TTQ model compounds. A non-linear curve-fitting program (Mac curve fit) was used to determine the rate constants in case the final value of the absorbance (A_∞) was obscured by the follow-up reaction.

Catalytic Oxidation. The catalytic oxidation of benzylamine (100 mM) by **1** (1 mM) was carried out in the presence of a metal ion in CH_3CN under O_2 atmosphere at 25 °C for 24 h. The ^1H NMR (JEOL FT-NMR GX-400) and IR (Shimadzu FTIR-8200PC) spectra of the concentrated final reaction mixture indicated that *N*-benzylideneben-zylamine ($PhCH_2N{=}CHPh$) was formed quantitatively; ^1H NMR ($CDCl_3$) δ 4.80 (2H, s, $-CH_2$-), 7.20−7.50 (8H, m, aromatic protons), 7.70−7.85 (2H, m, aromatic protons), 8.38 (1H, br s, $-CH{=}$); IR (neat) 1648 cm^{-1} (C═N).

Electrochemical Measurements. The cyclic voltammetry (CV) measurements were performed on a BAS 100B or an ALS 600 electrochemical analyzer in anhydrous CH_3CN containing 0.10 M NBu_4PF_6 as a supporting electrolyte. The organic solvent was dried over CaH_2 and distilled just before use for the experiments. The Pt working electrodes were polished with a polishing alumina suspension and rinsed with acetone before use. The counter electrode was a Pt wire. An Ag/$AgNO_3$ electrode or a silver wire was used as a reference electrode. When the silver pseudo reference electrode was used, the potentials were referenced vs the ferrocene/ferricenium couple. All electrochemical measurements were carried out at 25 °C under an atmospheric pressure of nitrogen.

Thin-layer UV−visible spectra of the electrochemically generated radical anions were taken by using a 0.5 mm path length quartz cell connected to the bottom of a three-necked vessel (ca. 20 mL capacity). An optically transparent platinum thin-layer electrode, which was placed in the quartz cell, was used as the working electrode and silver wires were used as counter and reference electrodes. Bulk electrolysis of **2** (6.0×10^{-4} M) was carried out at -0.5 V vs Ag/Ag^+ in anhydrous DMSO containing 0.1 M NBu_4PF_6 at 25 °C. UV−visible spectra were recorded on a Hewlett-Packard 8453 photodiode array spectrophotom-eter.

ESR Measurements. ESR spectra of the semiquinone radical anions of TTQ model compounds were taken on a JEOL JES-ME-2X. Details about the experimental conditions are given in the figure captions. The *g* values were determined using a Mn^{2+} marker as a reference. Computer simulation of the ESR spectra was carried out by using ESRaII version 1.01 (Calleo Scientific Publisher) on a Macintosh personal computer.

Theoretical Calculations. The theoretical studies were performed using the PM3 method.[23] The calculations were performed by using a MOL-MOLIS program Ver. 2.8 (Daikin Industries, Ltd) or a Spartan program (Version 4.1, Wavefunction, Inc.). Final geometries and energetics were obtained by optimizing the total molecular energy with respect to all structural variables. The geometries of the radicals were optimized using the unrestricted Hartree−Fock (UHF) formalism.

Results and Discussion

Metal Ion Binding under Neutral Conditions. In Figure 1A−D are shown the spectral changes for the titrations of **1** by $Li(ClO_4)$, $Mg(ClO_4)_2$, $Ca(ClO_4)_2$, and $Sc(OTf)_3$, respectively. When **1** was treated with $Li(ClO_4)$ in anhydrous CH_3CN, the absorption band at 408 nm due to the quinone shifted to 430 nm and a broad absorption band appeard at 626 nm as shown in Figure 1A.[24] Essentially the same spectral change was observed in the titration with $Na(ClO_4)$ (Table 1). Because of the low solubility of $NH_4(ClO_4)$, $K(ClO_4)$, $Cs(ClO_4)$, and Cs(OTf) in CH_3CN, an interaction between **1** and those monovalent cations could not be examined accurately. The complexes of **1** with divalent metal cations, Mg^{2+} and Ca^{2+}, gave the more red-shifted absorption bands (Figure 1B,C) as compared to the monovalent cations (see λ_{max} values in Table 1).[24] The spectral change becomes more prominent for trivalent metal cations and in particular the Sc^{3+} complex gives the two absorption maxima at 489 and 802 nm (Figure 1D) which are the most red-shifted among the metal ions employed in this study.

The binding constant K_{ML} for 1:1 complex formation between the quinone (Q) and the metal ion (M^{n+}) can be expressed by eq 2, where A_0 and A_∞ are the initial and final absorptions of

$$\frac{A - A_0}{A_\infty - A} = K_{ML}\left([M^{n+}]_0 - \frac{A - A_0}{A_\infty - A_0}[Q]_0\right) \qquad (2)$$

the titration and $[M^{n+}]_0$ and $[Q]_0$ denote the concentration of the added metal ion and the initial quinone concentration, respectively.[25] Thus, the plot of $(A - A_0)/(A_\infty - A)$ vs $([M^{n+}]_0 - \alpha[Q]_0)$ $[\alpha = (A - A_0)/(A_\infty - A_0)]$ gives a straight line passing through the origin as shown in the insets of Figure 1, from which the K_{ML} values were obtained as the slopes. The K_{ML} values thus determined are listed in Table 1 together with the λ_{max} of the complex generated in the solution.

The *N*-methyl derivative **2** exhibited essentially the same spectral changes in the titration with the mono-, di-, and trivalent metal ions as those obtained for **1** (see λ_{max} values in Table 1).[24] In addition, the K_{ML} values of **2** with the divalent and trivalent cations were larger than those of **1** (Table 1), demonstrating that the *N*-methyl group at the 1-position does not hamper the metal ion binding but rather enhances the binding by its electron-donating nature. This indicates that the binding positions of the metal ions are the same for both quinones (**1** and **2**) and that the pyrrole nitrogen (N(1)) of the indolequinone ring does not participate directly as the metal ion-binding site.

The binding constants K_{ML} of the 4-phenyl- and 4-methylin-dolequinone derivatives, **3** and **4**, toward the metal ions were also determined in a similar manner. These results are also listed in Table 1 together with the λ_{max} of the 1:1 complexes. It should be noted that, in the case of **3**, the magnitude of the red-shift

(23) The PM3 method; Stewart, J. J. P. *J. Comput. Chem.* **1989**, *10*, 209, 221.

(24) The λ_{max} values of the broad absorption band in the NIR region were determined using subtraction spectra (final spectrum − initial spectrum) in case the λ_{max} was obscure. No spectral change was observed in *methanol* with any metal ions under the same experimental conditions.

(25) Itoh, S.; Kawakami, H.; Fukuzumi, S. *Biochemistry* **1998**, *37*, 6562−6571.

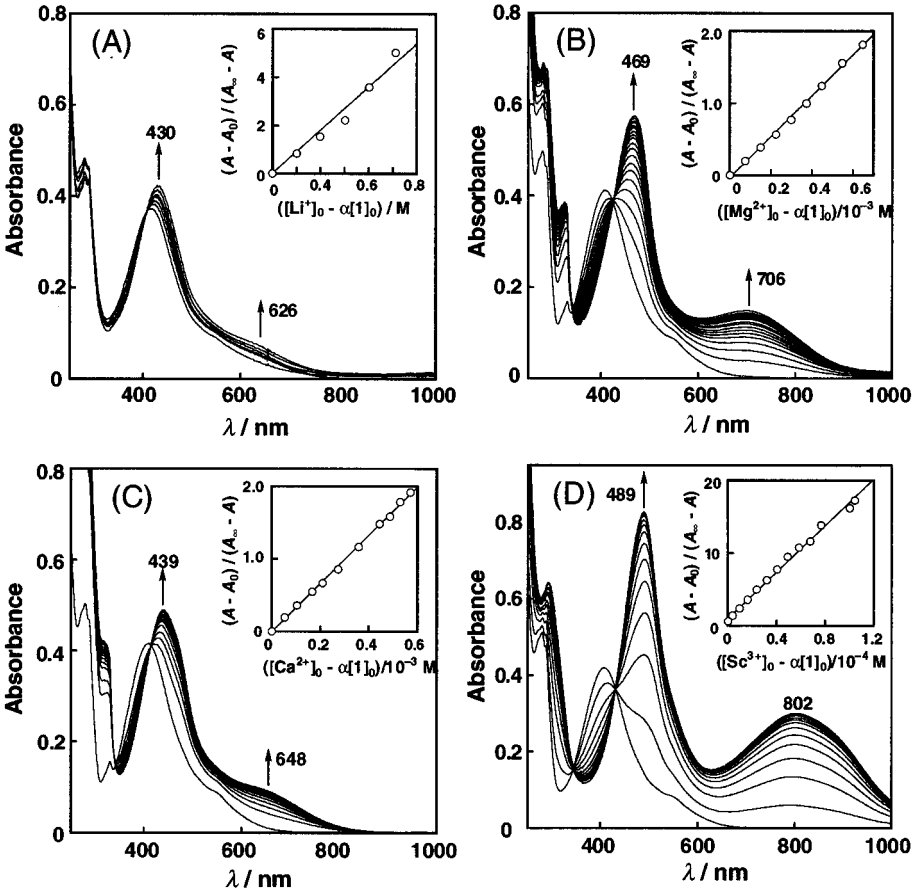

Figure 1. Spectral changes observed upon addition of (A) $LiClO_4$ (0−1.87 M), (B) $Mg(ClO_4)_2$ (0−5.75 × 10^{-2} M), (C) $Ca(ClO_4)_2$ (0−4.0 × 10^{-2} M), and (D) $Sc(OTf)_3$ (0−1.5 × 10^{-3} M) to a CH_3CN solution of **1** (5 × 10^{-5} M) at 25 °C. Insets: Plot of $(A - A_0)/(A_\infty - A)$ vs $[M]_0 - \alpha[\mathbf{1}]_0$ [$\alpha = (A - A_0)/(A_\infty - A_0)$].

Table 1. Binding Constants (K_{ML}) of the Metal Ions to the TTQ Model Compounds and the λ_{max} Values of the Quinone and the Metal Complexes in CH_3CN at 25 °C

		λ_{max}/nm		
quinone	metal ion	quinone	complex	K_{ML}/M^{-1}
1	Li^+	408	430, 626	4.5
1	Na^+	408	425, 619	2.3
1	Mg^{2+}	408	469, 706	136
1	Ca^{2+}	408	439, 648	327
1	Sr^{2+}	408	431, 641	185
1	Ba^{2+}	408	430, 631	164
1	Sc^{3+}	408	489, 802	166000
1	Y^{3+}	408	473, 718	441
1	Lu^{3+}	408	478, 733	657
2	Li^+	413	431, 611	2.9
2	Mg^{2+}	413	467, 693	252
2	Ca^{2+}	413	442, 638	525
2	Sc^{3+}	413	487, 792	427000
3	Li^+	400	416, 568	3.4
3	Mg^{2+}	400	442, 580	77
3	Ca^{2+}	400	430, 578	207
3	Sc^{3+}	400	452, 694	21900
4	Li^+	391	411	4.8
4	Na^+	391	403	2.5
4	Mg^{2+}	391	433	167
4	Ca^{2+}	391	423	318
4	Sc^{3+}	391	459	96700

and the absorption intensity of the broad peak in NIR region of the metal ion complexes became significantly small as compared to those of **1** and **2**, and that no NIR absorption band is observed in the case of 4-methyl derivative **4** (see Table 1). In Figure 2A,B are shown the spectral changes observed in the titrations of **3** and **4** with Sc^{3+} as typical examples. Such a small and almost no spectral change in the NIR region in the cases of **3** and **4**, respectively, indicates that the board absorption bands appearing in the NIR region are due to an *intramolecular charge transfer* from the aromatic rings at the 4-position to the quinone moiety. The intramolecular charge transfer may occur more efficiently from the electron rich indole ring in **1** and **2** than from the phenyl ring in **3**, and such an intramolecular charge transfer is not expected to occur from the methyl group in **4**. In fact, the charge-transfer transition energy ($h\nu_{CT}$) is well correlated with the binding strength of metal ions to **1** and **2** as shown in Figure 3, where a linear correlation is observed between the free energy change for formation of the metal ion complex ($\Delta G_{ML} = -RT \ln K_{ML}$) and the $h\nu_{CT}$ values.

Despite our great efforts, a single crystal of the metal ion complexes suitable for X-ray crystallographic analysis could not be obtained. Thus, we examined the binding position of the metal ion to the quinone using ^1H and ^{13}C NMR. Since the binding of Sc^{3+} to the quinones is exceptionally strong, the NMR study was carried out on the Sc^{3+} complex of **1** in CD_3CN (Table 2). In the ^1H NMR spectrum, the methyl protons at the 3-position and the vinyl proton at the 5-position move downfield by the complexation with Sc^{3+} ($\Delta\delta = +0.32$ and $+0.30$ ppm, respectively) and the downfield shift of the acidic pyrrole proton at the 1-position is more significant ($\Delta\delta = +1.25$ ppm). In the ^{13}C NMR spectrum, the quinone carbonyl carbon at the 7-position shifted downfield ($\Delta\delta = +3.1$ ppm), while the quinone carbonyl carbon at the 6-position shifted upfield by the complexation with Sc^{3+} ($\Delta\delta = -1.5$ ppm). These results can be explained by the interaction of Sc^{3+} with the quinone

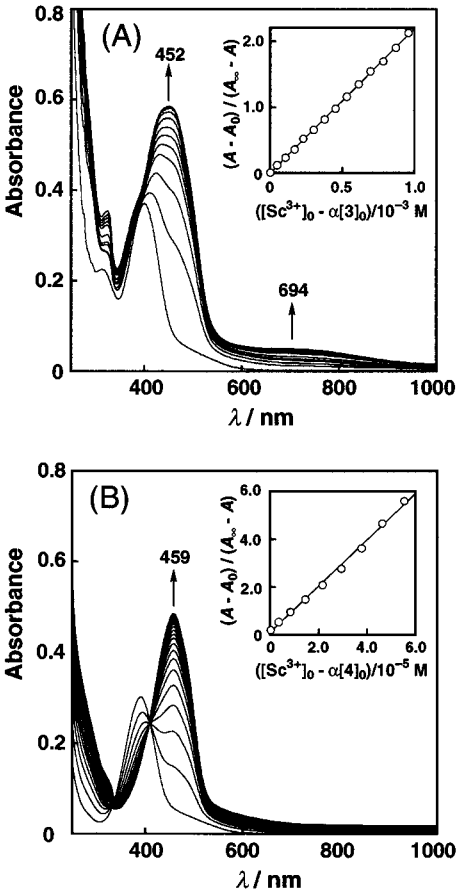

Figure 2. (A) Spectral change observed upon addition of $Sc(OTf)_3$ ($0-1.15 \times 10^{-3}$ M) to a CH_3CN solution of **3** (5×10^{-5} M) at 25 °C. Inset: Plot of $(A - A_0)/(A_\infty - A)$ vs $[Sc(OTf)_3]_0 - \alpha[\mathbf{3}]_0$ [$\alpha = (A - A_0)/(A_\infty - A_0)$]. (B) Spectral change observed upon addition of $Sc(OTf)_3$ ($0-2.0 \times 10^{-4}$ M) to a CH_3CN solution of **4** (5×10^{-5} M) at 25 °C. Inset: Plot of $(A - A_0)/(A_\infty - A)$ vs $[Sc(OTf)_3]_0 - \alpha[\mathbf{4}]_0$ [$\alpha = (A - A_0)/(A_\infty - A_0)$].

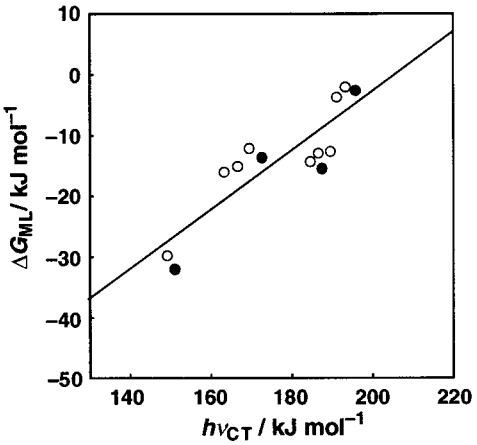

Figure 3. Plot of ΔG_{ML} vs $h\nu_{CT}$ for the complex formation between **1** (○) and **2** (●) with the metal ions at 25 °C in anhydrous acetonitrile.

carbonyl oxygens [O(6) and O(7)]. Since the pyrrole proton at the 1′-position and the methyl protons at the 3′-position of the second indole ring also move downfield ($\Delta\delta = +0.24$ and $+0.20$, respectively), the electronic effect resulting from the complex formation extends to the whole molecule. On the other hand, the methyl group at the 1-position in **2** has little effect on the binding constant (K_{ML}) for any metal ions (Table 1). This indicates that there is no direct interaction between the metal ions and the pyrrole nitrogen at the 1-position.

Table 2. Selected ^1H and ^{13}C NMR Data of **1** and Its Sc^{3+} Complex in CD_3CN

		δ/ppm	
	nucleus	**1**	**1**-Sc^{3+}
^1H NMR	H-1	10.35	11.60
	H-2	6.94	—[a]
	CH_3-3	1.56	1.88
	H-5	5.91	6.21
	H-1′	9.32	9.56
	CH_3-3′	2.34	2.54
^{13}C NMR	CH_3-3	10.7	13.1
	C-6	168.6	167.1
	C-7	184.1	187.2
	CH_3-3′	9.4	11.6

[a] Could not be determined because of the overlap with the large solvent peak.

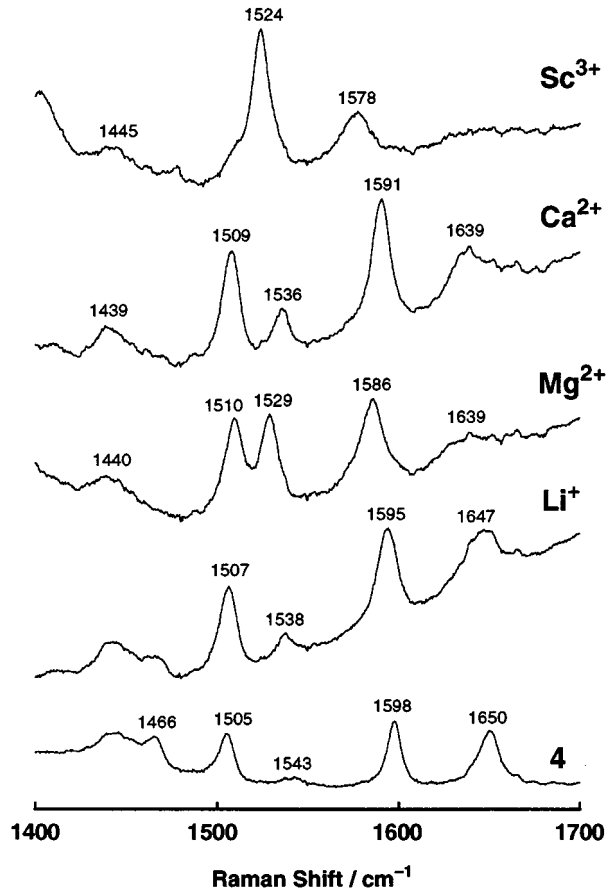

Figure 4. Resonace Raman spectra obtained with 413.1 nm excitation of **4** (0.5 mM) alone and in the presence of $LiClO_4$ (0.92 M), $Mg(ClO_4)_2$ (0.40 M), $Ca(ClO_4)_2$ (0.34 M), and $Sc(OTf)_3$ (3.0×10^{-3} M) in CH_3CN at 25 °C; The laser power used was 16 mW at the sample point. Exposure times are 2 or 4 s for the Sc^{3+}, Ca^{2+}, Mg^{2+}, and Li^+ complexes and 10 s for **4** alone. Total accumlations are 100 times for the Sc^{3+}, Ca^{2+}, Mg^{2+}, and Li^+ complexes and 20 times for **4** alone.

Resonance Raman measurements were carried out for a series of metal ion complexes of the model compounds, since it would provide unique structural information on the quinone cofactor.[17,18] Figure 4 shows resonance Raman spectra of the metal ion complexes of quinone **4** and its metal-free form. The Raman bands in the 1400−1700 cm^{-1} region are mainly associated with C═O and C═C stretching modes, although they are strongly mixed. These bands are primarily influenced by complex formation with the metal ions. Particularly, the Mg^{2+} and Sc^{3+} complexes are significantly altered. The band around 1650 cm^{-1}, which contains larger contribution from the quinone carbonyl

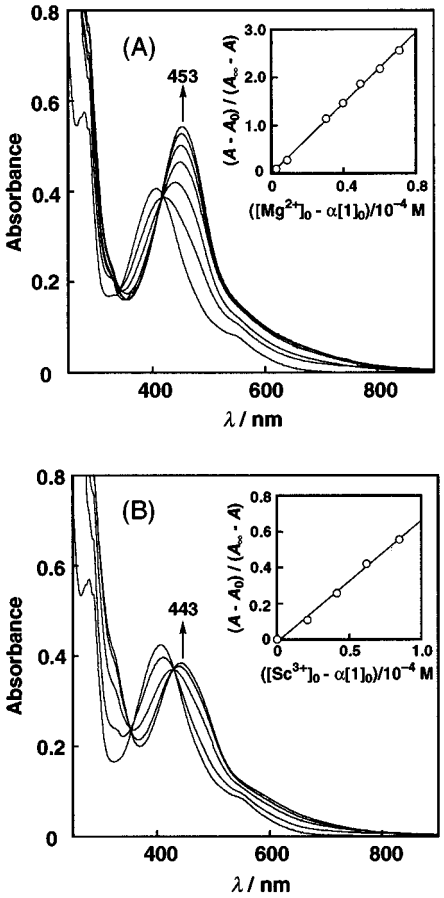

Figure 5. Spectral changes observed upon addition of (A) $Mg(ClO_4)_2$ ($0-1.5 \times 10^{-4}$ M) and (B) $Sc(OTf)_3$ ($0-2.5 \times 10^{-4}$ M) to a CH_3CN solution of **1** (5.0×10^{-5} M) in the presence of 0.01 M benzylamine at 25 °C. Inset: Plot of $(A - A_0)/(A_\infty - A)$ vs $[M]_0 - \alpha[\mathbf{1}]_0$ [$\alpha = (A - A_0)/(A_\infty - A_0)$].

Chart 1

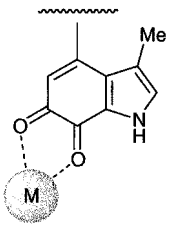

stretching mode,[18] is shifted to lower frequencies and significantly broadened when the metal coordination is strong. As the complexation becomes stronger, double bond character of the C═O bonds decreases and then they would lose resonance enhancement of Raman intensity. Although detailed assignment of the Raman bands has yet to be made, the Raman spectral changes indicate that the metal ion coordination occurs at the quinone group, in agreement with the results of NMR measurements (vide supra). Taking all the spectroscopic data into account, the structure of the complex is proposed as illustrated in Chart 1.

Metal Ion Binding under Basic Conditions. Coordination of metal ions to the quinones has been examined in the presence of an amine, before examining the catalytic effects of the metal ions on the amine-oxidation. In Figure 5 are shown the spectral changes of the titration of **1** with $Mg(ClO_4)_2$ and $Sc(OTf)_3$ in the presence of benzylamine as typical examples.[26] The spectral change for the titration of **1** with $Ca(ClO_4)_2$ was essentially the same to that of the titration of **1** with $Mg(ClO_4)_2$. Each spectrum was taken immediately after the addition of the metal ion, since the redox reaction between **1** and benzylamine gradually occurred at a prolonged reaction time (vide infra). The absorption band at 408 nm due to the quinone itself decreases with an increase in the intensity in a new absorption band of the complex, when the concentration of added metal ion was increased. The binding constants K_{ML} for 1:1 complex formation between the quinones (Q) and the metal ions (M^{n+}) have also been determined using eq 2, and they are summarized in Table 3 together with the λ_{max} values of the quinones and the metal complexes.

Table 3. Binding Constants (K_{ML}) of the Metal Ions to the Quinones and the λ_{max} Values of the Quinones and the Metal Complexes in the Presence of Benzylamine (0.01 M) in CH_3CN at 25 °C

		λ_{max}/ nm		
quinone	metal ion	quinone	complex	K_{ML}/M^{-1}
1	Li^+	408	463	15.6
1	Na^+	408	454	5.5
1	Mg^{2+}	408	453	36700
1	Ca^{2+}	408	458	247000
1	Sr^{2+}	408	473	340000
1	Ba^{2+}	408	476	397000
1	Sc^{3+}	408	443	6760
2	Li^+	413	435	3.6
3	Li^+	400	456	10.7
3	Mg^{2+}	400	454	19700
3	Ca^{2+}	400	459	122000
4	Li^+	391	447	16.0
4	Mg^{2+}	391	445	46000
4	Ca^{2+}	391	455	229000

The binding constants K_{ML} for the monovalent and divalent cation complexes with **1**, **3**, and **4** in the presence of benzylamine (Table 3) are significantly larger than those in its absence (Table 1), whereas no effect of the base is observed for the Li^+ complex of quinone **2**. The larger the ionic radius (Mg^{2+} 0.66 Å; Ca^{2+} 0.99 Å; Sr^{2+} 1.12 Å; Ba^{2+} 1.34 Å), the greater the K_{ML} value ($Mg^{2+} < Ca^{2+} < Sr^{2+} < Ba^{2+}$) in the presence of benzylamine (Table 3). The increase in K_{ML} value in the presence of benzylamine may be due to the deprotonation of the pyrrole proton at the 1-position (1-NH), which generates a negative charge on the indolequinone ring and attracts the cationic species more strongly. In fact, the pyrrole proton signal (e.g., $\delta = 11.60$ of the Sc^{3+} complex of **1** in CD_3CN) completely disappeared when benzylamine was added into the solution. Disappearance of the NIR absorption in the presence of the base (Figure 5 and Table 3) is also ascribed to the dissociation of the pyrrole proton, the negative charge generated by which precludes the intramolecular charge transfer from the C-4 aromatic group to the quinone moiety of TTQ. In the case of the 1-Me derivative **2**, which has no dissociable pyrole proton, the binding with the metal ion is not affected by the presence of the benzylamine base.

In contrast to the case of monovalent and divalent metal ions, the K_{ML} values of the trivalent cation complexes of **1** in the presence of the base (Table 3) are significantly smaller than those in its absence (Table 1). Trivalent metal ions such as Sc^{3+} have strong affinity toward heteroatoms (O and N) as indicated by the large K_{ML} values in Table 1. In the presence of benzylamine, however, a strong interaction between Sc^{3+} and the added amine may result in a significant decrease of the affinity toward the quinone itself.

(26) The spectral change for the titration of **1** with $Li(ClO_4)$ in the presence of benzylamine has been reported already.[20]

Scheme 2

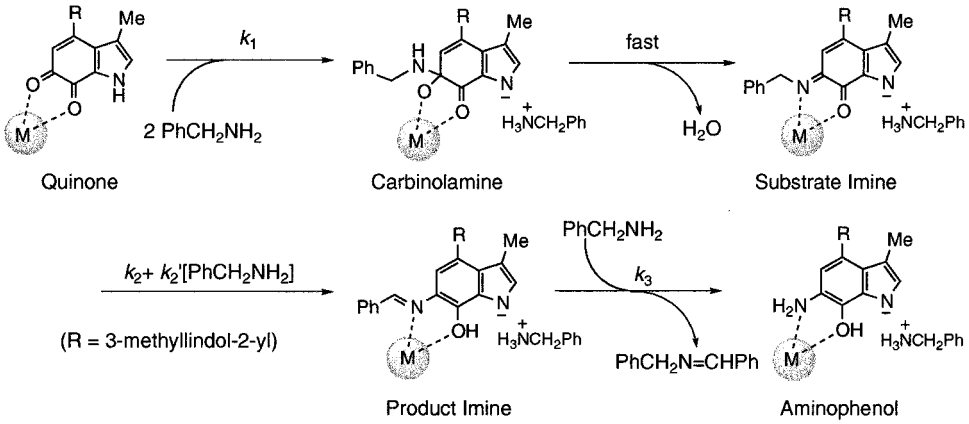

The spectral changes of the titrations with various metal ions in the presence of benzylamine are fairly close each other, suggesting that the binding site of the metal ions is basically the same in all the metal ion systems (*o*-quinone moiety). In enzymatic systems, however, alkaline metal ions cause a decrease in absorbance of the peak at 455 nm and the broad band at around 600−800 nm and an appearance of a shoulder at ca. 340 nm.[27] Zhu and Davidson proposed that this spectral change is due to chemical modification of TTQ to form a hydroxide adduct.[27] If so, it can be concluded that nucleophilic addition of benzylamine to the quinone (k_1 process in Scheme 2, vide infra) does not occur just after the addition of amine to the metal ion complex of quinone in anhydrous CH_3CN.

Metal Ion-Catalyzed Oxidation of Benzylamine by TTQ Model Compounds. We have previously reported that benzylamine is oxidized by TTQ model compound **1** in CH_3OH via a transamination mechanism, which consists of three distinctive steps: addition of the amine to the quinone (k_1), the spontaneous (k_2) and the amine-catalyzed (k_2') rearrangement from the substrate imine to the product imine intermediates, and the imine exchange reaction (k_3) to generate the aminophenol and *N*-benzylidenebenzylamine ($PhCH_2N{=}CHPh$) (cf. Scheme 2).[9,10] The reaction intermediates (substrate imine and product imine) and the aminophenol products have been isolated and characterized in the reaction of **1** with various amines in CH_3OH.[9,10] When methanol is replaced by an aprotic solvent such as anhydrous CH_3CN, however, even adduct formation (k_1 process) does not take place between benzylamine and **1**.[28] Strong solvation of protic solvents such as CH_3OH to the quinone may be required to enhance the electrophilicity of the quinone moiety of the model compound, making it possible to undergo the oxidation of benzylamine.

Metal ions can also enhance the electrophilicity of **1** by the complexation. Thus, the reaction of quinone **1** (5.0×10^{-5} M) and benzylamine (1.5×10^{-2} M) in the presence of $LiClO_4$ (0.15 M) in anhydrous CH_3CN at 25 °C under anaerobic conditions resulted in a drastic spectral change where the absorption band at 463 nm due to the Li^+ complex of the quinone decreases, accompanied by an increase in a new band at 323 nm due to the reduced TTQ in the aminophenol form as shown in Figure 6.[29] The spectral change in the metal ion-catalyzed oxidation of benzylamine by **1** is essentially the same as reported for the reaction in CH_3OH,[9,10] when the well-established three steps can be followed in different time scales. The first step (Figure 6A) corresponds to addition of the amine to the quinone (k_1), the second step (Figure 6B) is due to the spontaneous (k_2) and the amine-catalyzed (k_2') rearrangement from the substrate imine to the product imine intermediates, and the final and the slowest step (Figure 6C) is ascribed to the imine exchange reaction (k_3) to generate the aminophenol and *N*-benzylidenebenzylamine ($PhCH_2N{=}CHPh$) as summarized in Scheme 2. Each process has its own isosbestic point at 418, 383, and 372 nm, respectively, confirming the validity of the stepwise mechanism in Scheme 2. Since the difference in the rate of each step was not large enough to determine the rate independently, the pseudo-first-order rate constants for three steps [$k_{obs(1)}$, $k_{obs(2)}$, and $k_{obs(3)}$] were determined simultaneously by computer simulation of the time course of the absorption change using a non-linear curve-fitting program (Mac curve fit) as reported in the previous study.[9,10] From the dependence of k_{obs} in each step on the amine concentration were determined the rate constants $k_1 = 5.9 \times 10^{-2}$ M^{-1} s^{-1}, $k_2 = 8.7 \times 10^{-5}$ s^{-1}, $k_2' = 2.6 \times 10^{-2}$ M^{-1} s^{-1}, and $k_3 = 1.4 \times 10^{-2}$ M^{-1} s^{-1} as shown in the insets of Figure 6.

Table 4. Rate Constants for the Oxidation of Benzylamine by **1** in the Presence of Metal Ions in CH_3CN at 25 °C

M	[M]/M	k_1[a]/M^{-1} s^{-1}	k_2[a]/s^{-1}	k_2' [a]/M^{-1} s^{-1}	k_3[a]/M^{-1} s^{-1}
Li^+	0.15	5.9×10^{-2}	8.7×10^{-5}	2.6×10^{-2}	1.4×10^{-2}
Mg^{2+}	1.5×10^{-3}	1.3	7.7×10^{-4}	1.1×10^{-1}	5.1×10^{-2}
Ca^{2+}	1.0×10^{-2}	0.40	3.9×10^{-4}	2.6×10^{-2}	3.9×10^{-2}
Sc^{3+}	5.0×10^{-4}	16.3	2.7×10^{-3}	1.28	1.5×10^{-1}

[a] The experimental error is within ±5%.

The oxidation of benzylamine by **1** proceeds more efficiently in the presence of the di- and trivalent metal ions (M^{2+} and M^{3+}). In all cases, the reaction consisted of three distinct steps [$k_{obs(1)}$, $k_{obs(2)}$, and $k_{obs(3)}$] as in the case of Li^+, and the rate constants for each process (k_1, k_2, k_2', and k_3) were determined from the dependence of the k_{obs} value of each step on the amine concentration as described above (Table 4). All the rate constants, k_1, k_2, k_2', and k_3, were nearly independent of the metal ion concentrations, confirming that the metal ion complex of **1** is the reactive species in the amine oxidation reaction. A relation between the rate constants [log(k_1, k_2, k_2', and k_3)] and the binding constant (logK_{ML}) in Table 1 is shown in Figure 7.

(27) Zhu, Z.; Davidson, V. L. *Biochem. J.* **1998**, *329*, 175−182.

(28) A simple *o*-quinonoid compound such as 3,5-di-*tert*-butyl-1,2-benzoquinone has been reported to undergo transamination reaction in an aprotic solvent such as chloroform (Klein, R. F. X.; Bargas, L. M.; Horak, V. *J. Org. Chem.* **1988**, *53*, 5994−5998). Less reactivity of the TTQ model compounds toward nucleophilic addition of amines may be due to the electron-donating nature of the conjugated pyrrole and the indolyl and alkyl substituents at the 4-position.

(29) Even though the transamination reaction of benzylamine by **1** proceeds in methanol,[9,10] addition of the metal ion into the methanol solution of **1** and benzylamine does not accelerate the reaction beteen them.

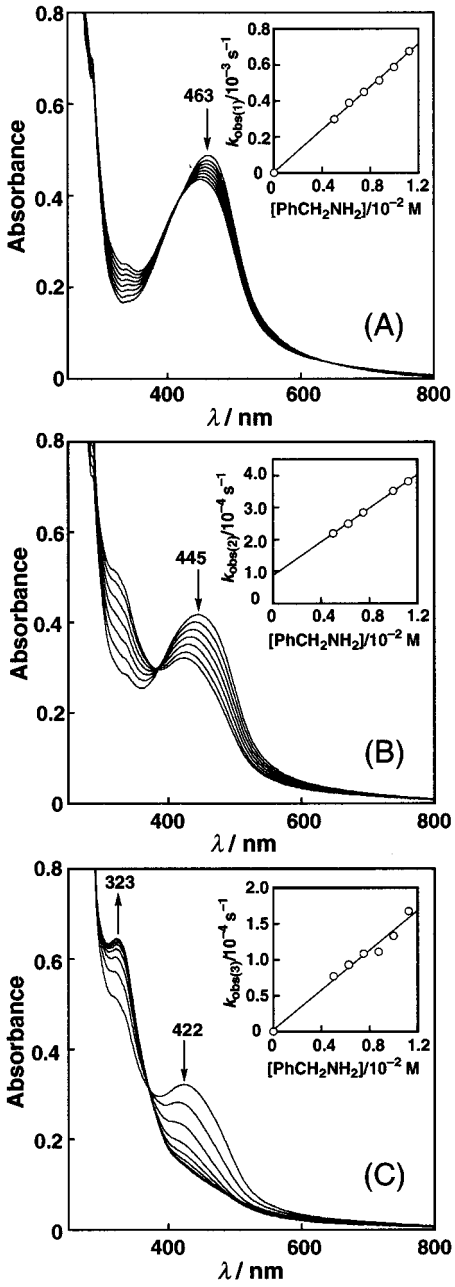

Figure 6. Spectral changes for the reaction of **1** (5.0×10^{-5} M) with benzylamine (1.5×10^{-2} M) in the presence of $LiClO_4$ (0.15 M) in anhydrous CH_3CN at 25 °C under anaerobic conditions: (A) the first stage (0−7200 s), 800 s interval (Inset: plot of $k_{obs(1)}$ vs [$PhCH_2NH_2$]); (B) the second stage (9600−24000 s), 2400 s interval (Inset: plot of $k_{obs(2)}$ vs [$PhCH_2NH_2$]); and (C) the third stage (24000−49600 s), 3200 s interval (Inset: plot of $k_{obs(3)}$ vs [$PhCH_2NH_2$]).

Each rate constant increases similarly with an increase in the positive charge of the metal ion: monovalent metal ion (Li^+) < divalent metal ion (Mg^{2+}, Ca^{2+}) < trivalent metal ion (Sc^{3+}) as the K_{ML} value also increases with the same order. In the case of divalent metal ions, however, each rate constant for the Mg^{2+}-catalyzed reaction is larger than that for the Ca^{2+}-catalyzed reaction whereas the K_{ML} value of the Mg^{2+} complex is smaller than that of the Ca^{2+} complex (Figure 7). Such a difference between the rate constants and the binding constants may be ascribed to the difference in the coordination sites between the binding to the reactant **1** and the intermediates in Scheme 2.

It also should be emphasized that the oxidation of benzylamine by the metal ion complex of **1** proceeds catalytically,

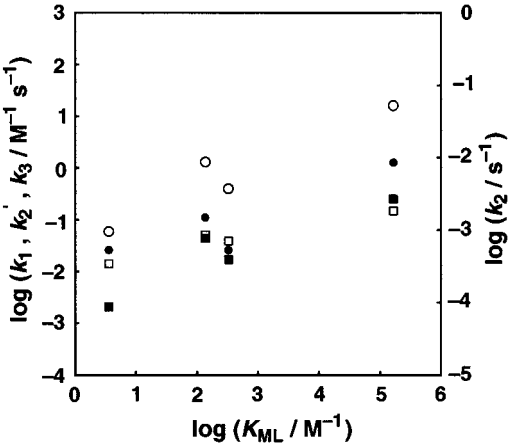

Figure 7. Plots of logk_1 (○), logk_2 (■), logk_2'(□), and logk_3 (●) against logK_{ML} for the oxidation of benzylamine by **1** catalyzed by the metal ions (Li^+, Mg^{2+}, Ca^{2+}, and Sc^{3+}).

Table 5. Rate Constants for the Oxidation of Aliphatic Amines by **1** in the Presence of Sc^{3+} (5.0×10^{-4} M) in CH_3CN at 25 °C

amine	k_1[a]/M^{-1} s^{-1}	k_2[a]/s^{-1}	k_2' [a]/M^{-1} s^{-1}	k_3[a]/M^{-1} s^{-1}
n-propylamine	38.7	7.5×10^{-3}	0.35	8.1×10^{-2}
n-hexylamine	11.2	5.3×10^{-3}	0.28	1.0×10^{-1}
isopropylamine	7.1	5.6×10^{-3}	0.24	

[a] The experimental error is within ±5%.

when molecular oxygen is used as an electron acceptor to regenerate the iminoquinone form from the reduced TTQ. Thus, benzylamine (0.10 M) was converted into *N*-benzylidenebenzylamine quantitatively, when it was treated with a catalytic amount of **1** (1.0×10^{-3} M; 1 mol %) in the presence of $LiClO_4$ (1.0 M) under aerobic conditions for 24 h.

Catalysis of Metal Ions on Oxidation of Aliphatic Amines. In contrast to the case of benzylamine, no redox reaction occurs between **1** and aliphatic amines even in CH_3OH. However, addition of Sc^{3+} into a CH_3CN solution of **1** and an aliphatic amine such as *n*-propylamine, *n*-hexylamine, or isopropylamine resulted in the spectral changes due to the redox reaction of the quinone. The reactions with aliphatic amines also consist of three distinct steps that can be similarly attributed to the addition of the amine to the quinone (k_1), the spontaneous (k_2) and the amine-catalyzed (k_2') rearrangement from the substrate imine to the product imine, and the imine exchange reaction (k_3) to generate the aminophenol and $RCH_2N{=}CHR$, respectively (Scheme 2). In the case of isopropylamine, however, the third step (k_3) is very slow. The rate constants of each process were determined in a similar manner as described above and are listed in Table 5. For the addition step of the amine (k_1), *n*-propylamine is most reactive, which may be due to the less steric hindrance of the short *n*-alkyl group as compared to the other substituents such as *n*-hexyl, secondary alkyl, and benzyl. The smaller reactivity of aliphatic amines in the base-catalyzed rearrangement (k_2') can be explained by the fact that the acidity of the α-proton of aliphatic amines is smaller than that of benzylamine. The primary amines show a similar reactivity in the third process (k_3) although reactivity of the secondary amine in this process is significantly suppressed probably due to the steric hindrance by the secondary alkyl group of the amine.

Effects of Metal Ions on the Redox Properties of TTQ Model Compounds. It has been reported that the semiquinone radical anion of TTQ in the enzyme active site is significantly stabilized by the interaction with the cationic species.[16] It has also been demonstrated that the electron transfer from the reduced TTQ to amicyanin is controlled by the interaction with

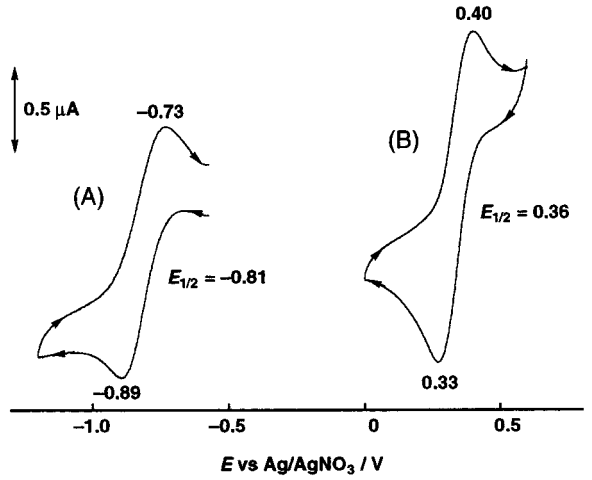

Figure 8. Cyclic voltammograms of **1** (1.0×10^{-3} M) alone (A) and in the presence of $Mg(ClO_4)_2$ (1.0×10^{-2} M) (B) containing 0.1 M Bu_4NPF_6 in anhydrous CH_3CN at 25 °C under anaerobic conditions: working electrode, Pt; counter electrode, Pt;, reference electrode, Ag/$AgNO_3$; scan rate, 10 mVs^{-1}

a cationic species.[19] Thus, we examined the effects of metal ions on the one-electron reduction potentials (E^0_{red}) of TTQ model compounds by the electrochemical methods. We have previously reported that TTQ model compound **1** shows a reversible redox couple at −0.188 V vs SCE in an aqueous buffer solution at pH 7.4.[8] This redox couple corresponds to two-electron redox reaction between the quinone and the quinol, and its value is fairly close to that of native MADH ($E_{1/2}$ = −0.148 V vs SCE at pH 7.5).[30] In anhydrous CH_3CN, on the other hand, **1** shows a one-electron pseudoreversible redox couple at −0.81 V vs $Ag/AgNO_3$ (−0.52 V vs SCE)[31] as shown in Figure 8A. Thus, **1** is reversibly reduced into $\mathbf{1}^{\bullet-}$ in CH_3CN. Such a reversible wave indicates that there is no acid−base reaction between $\mathbf{1}^{\bullet-}$ and **1** in CH_3CN even though **1** itself has a dissociable pyrrole proton (1-NH) as does coenzyme PQQ.[32] It is interesting to note that the E^0_{red} value of **1** is about 0.2 V lower than that of 1-Me-PQQTME (1-methyl derivative of the trimethyl ester of coenzyme PQQ).[32] This may be mainly due to the electron-withdrawing effect of the pyridine nucleus having two ester groups of the PQQ model compound.

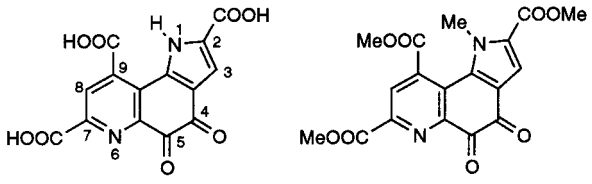

Although low solubility of monovalent cations such as ammonium and alkaline metal ions in anhydrous CH_3CN precluded detailed examination of their effects on the redox potential of **1**, the complex formation of **1** with the divalent and trivalent metal ions resulted in a significantly large positive shift of E^0_{red}. In Figure 8B is shown a cyclic voltammogram of **1** in the presence of Mg^{2+} in anhydrous CH_3CN. Addition of Mg^{2+} results in a remarkably large positive shift of E^0_{red} by 1.17 V. In the presence of Sc^{3+}, **1** also exhibited a reversible redox couple at 0.35 V vs $Ag/AgNO_3$, causing a similar large positive shift of E^0_{red} (ΔE^0_{red} = 1.16 V). In the case of Ca^{2+}, however, a much smaller positive shift of E^0_{red} (ΔE^0_{red} = 0.47 V) was observed. According to the Nernst equation, ΔE^0_{red} is determined by the difference in the binding constants between metal ion complexes with **1** ($K_{ML(ox)}$) and $\mathbf{1}^{\bullet-}$ ($K_{ML(red)}$) as given by eq 3. The $K_{ML(red)}$ values are then determined from the $K_{ML(ox)}$

$$\Delta E^0_{red} = RT \ln(K_{ML(red)}/K_{ML(ox)}) \qquad (3)$$

values in Table 1 using eq 3 as 2.9×10^{10}, 8.1×10^{21}, and 6.7×10^{24} M^{-1} for Ca^{2+}-$\mathbf{1}^{\bullet-}$, Mg^{2+}-$\mathbf{1}^{\bullet-}$, and Sc^{3+}-$\mathbf{1}^{\bullet-}$, respectively. The small ΔE^0_{red} value for the Ca^{2+}-$\mathbf{1}^{\bullet-}$ complex is therefore attributed to the small binding constant ($K_{ML(red)}$) as compared to those of the Mg^{2+} and Sc^{3+} complexes with $\mathbf{1}^{\bullet-}$. In contrast to the case of **1**, the smaller ionic radius of Mg^{2+} than Ca^{2+} favors the binding to $\mathbf{1}^{\bullet-}$.

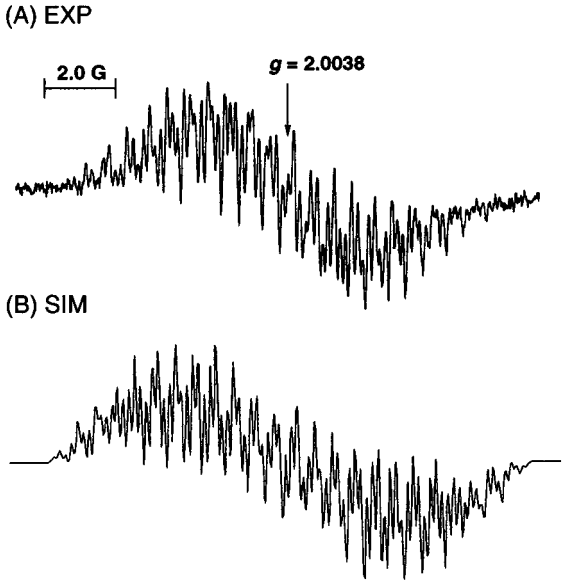

Figure 9. (A) ESR spectrum of $\mathbf{1}^{\bullet-}$ generated by half-reduction of **1** (5.0×10^{-3} M) with $MeNHNH_2$ (2.5×10^{-3} M) in the presence of NEt_3 (1.0 M) in CH_3OH at 25 °C under anaerobic conditions. (B) Computer simulation spectrum of $\mathbf{1}^{\bullet-}$, ΔH_1 = 0.035 G.

Semiquinone Radical Anions and the Metal Ion Complexes. Semiquinone radical anion $\mathbf{1}^{\bullet-}$ was generated by comproportionation of the quinone **1** and quinolate $\mathbf{1H}^-$ generated in situ by the half reduction of **1** (5.0×10^{-3} M) by $MeNHNH_2$ in the presence of NEt_3 in CH_3OH. Figure 9A shows a solution ESR spectrum of $\mathbf{1}^{\bullet-}$ measured at room temperature in CH_3OH together with the computer simulation spectrum. The *g* value is determined as 2.0038, which is within a range of those of ordinary semiquinone radical anions,[33] indicating the contribution of spin−orbit coupling due to electron spin partially localized at the oxygen nuclei. The observed hyperfine structure in Figure 9A is well reproduced by the computer simulation (Figure 9B) with the hyperfine splitting (hfs) values of eight nonequivalent protons (2.30, 1.16, 0.965, 0.56, 0.11, 0.06, 0.045,

(30) Burrows, A. L.; Hill, H. A. O.; Leese, T. A.; McIntire, W. S.; Nakayama, H.; Sanghera, G. S. *Eur. J. Biochem.* **1991**, *199*, 73−78.

(31) The $E_{1/2}$ values determined vs an $Ag/AgNO_3$ reference electrode and vs an Fc/Fc^+ electrode are converted to those vs SCE by adding 0.29 and 0.37 V, respectively; Mann, K.; Barnes, K. K. *Electrochemical Reactions in Nonaqueous Systems*; Marcel Dekker Inc.: New York, 1990.

(32) Itoh, S.; Kawakami, H.; Fukuzumi, S. *J. Am. Chem. Soc.* **1998**, *120*, 7271−7277.

(33) (a) Swarz, H. M.; Bolron, J. R.; Borg, D. C. *Biological Applicaton of Electron Spin Resonance*; John Wiley & Sons: New York, 1972; p 24. (b) Fukuzumi, S.; Nishizawa, N.; Tanaka, T. *J. Org. Chem.* **1984**, *49*, 3571.

Chart 2

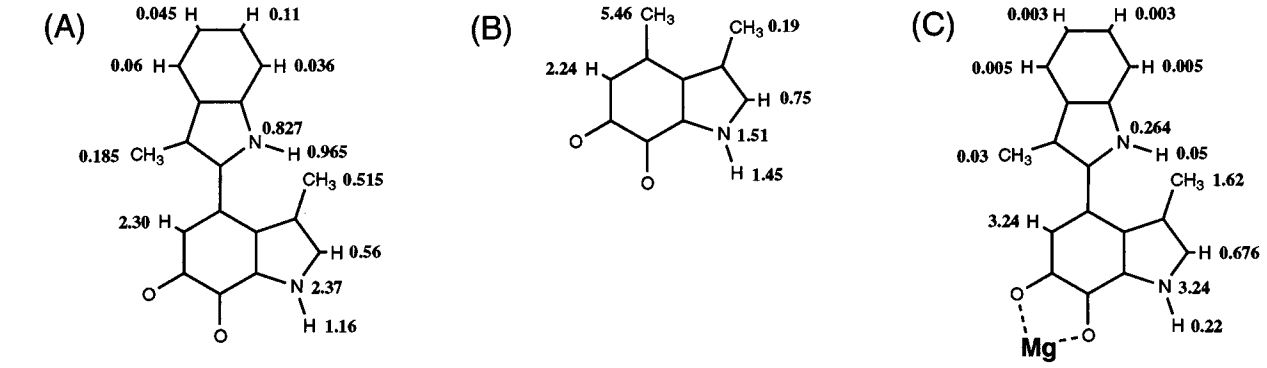

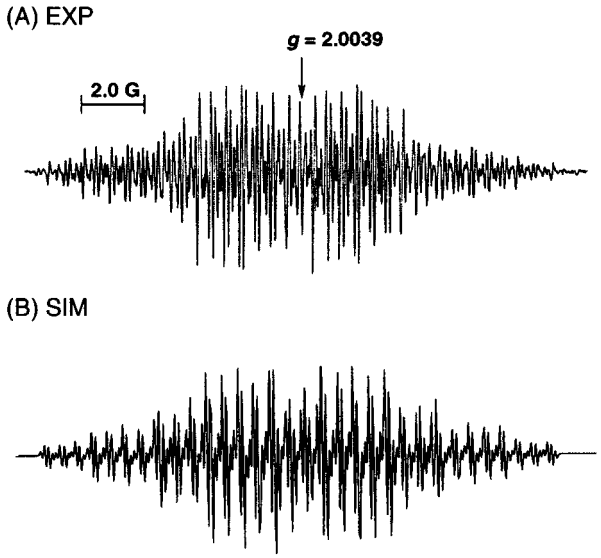

Figure 10. (A) ESR spectrum of $\mathbf{4}^{\bullet-}$ generated by half-reduction of **4** (5.0×10^{-3} M) with $MeNHNH_2$ (2.5×10^{-3} M) in the presence of NEt_3 (1.0 M) in CH_3OH under anaerobic conditions at −15 °C. (B) Computer simulation spectrum of $\mathbf{4}^{\bullet-}$, $\Delta H_1 = 0.05$ G.

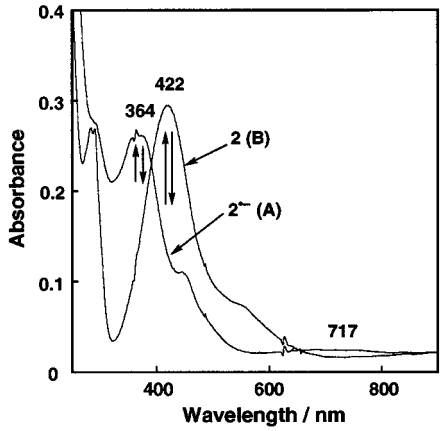

Figure 11. Spectral change during controlled potential electrolysis of **2** (6.0×10^{-4} M) at −0.5 V vs Ag wire containing 0.1 M Bu_4NPF_6 in anhydrous DMSO at 25 °C under anaerobic conditions: interval, 240 s.

and 0.036 G), two sets of methyl protons (0.515 and 0.185 G), and two nitrogen atoms (2.37 and 0.827 G).[34]

A solution ESR spectrum of $\mathbf{4}^{\bullet-}$ was also taken in a similar manner (Figures 10A). In the case of $\mathbf{4}^{\bullet-}$, however, lower temperature (−15 °C) was required for the ESR measurement because of the lower stability as compared with the quinone having the aromatic substituent at the 4-position such as $\mathbf{1}^{\bullet-}$. The *g* value of $\mathbf{4}^{\bullet-}$ (2.0039) is nearly the same as that of $\mathbf{1}^{\bullet-}$ (2.0038). The hyperfine structure is reproduced by the computer simulation (Figure 10B) with the hyperfine splitting (hfs) values of three nonequivalent protons (2.24, 1.45, and 0.75 G), two sets of methyl protons (5.46 and 0.19 G), and one nitrogen atom (1.51 G). Based on the calculated spin density of $\mathbf{1}^{\bullet-}$ and $\mathbf{4}^{\bullet-}$ by the PM3 method, we assigned those hfs values as shown in Chart 2.

It is interesting to note that a relatively large amount of the spin density is accumulated at the 4-position in $\mathbf{4}^{\bullet-}$ and delocalized into the aromatic rings in $\mathbf{1}^{\bullet-}$. This result is consistent with the proposal that the second indole ring connected at the 4-position of the indolequinone framework of TTQ acts as an electron-transfer route from the reduced TTQ to the copper site of electron-acceptor enzymes.[12]

Figure 11A shows the UV−vis spectrum of $\mathbf{2}^{\bullet-}$ generated by bulk electrolysis of **2** at −0.5 V vs Ag/Ag^+ in DMSO containing 0.1 M NBu_4PF_6. It has an intense absorption band at 364 nm together with a broad one at 717 nm. The blue shift of λ_{max} observed in the one-electron reduction of **2** has also been observed in the reduction of TTQ by dithionite in the enzymatic systems.[35,36] Bulk electrolysis of the resulting solution of $\mathbf{2}^{\bullet-}$ at 0.6 V vs Ag/Ag^+ regenerated quinone **2** quantitatively (Figure 11B), agreeing well with the reversibility observed in the cyclic voltammetric measurement (Figure 8).

The Mg^{2+} complex of semiquinone radical anion $\mathbf{1}^{\bullet-}$ was generated by comproportionation of the quinone **1** and quinolate $\mathbf{1H}^-$ in the presence of $Mg(ClO_4)_2$ in CH_3OH. The ESR spectrum of the Mg^{2+} complex of $\mathbf{1}^{\bullet-}$ is observed as shown in Figure 12A. The *g* value is determined as 2.0029, which is appreciably smaller than the *g* value of $\mathbf{1}^{\bullet-}$ (2.0038). The smaller *g* value of Mg^{2+}-$\mathbf{1}^{\bullet-}$ than that of $\mathbf{1}^{\bullet-}$ (2.0038) indicates that the spin density on oxygen nuclei in Mg^{2+}-$\mathbf{1}^{\bullet-}$ is decreased by the complexation with Mg^{2+}. The hyperfine structure can be reproduced by the computer simulation with the hyperfine splitting (hfs) values of eight protons (3.24, 0.676, 0.22, 0.05, 0.005, 0.005, 0.003, and 0.003 G), two sets of methyl protons (0.62 and 0.03 G), and two nitrogen atoms (3.24 and 0.264 G). Based on the calculated spin density of $\mathbf{1}^{\bullet-}$-Mg^{2+} by the PM3 method, we have tentatively assigned those hfs values as shown

(34) The resolution of the hyperfine structure has not been completely improved at a low field modulation down to 0.035 G.; the baseline of the spectrum is significantly undulated (Figure 9A). Such a limited resolution may be attributed to contribution of very small hyperfine splitting (hfs) values due to the aromatic protons of the second indole ring at the 4-position as well as a non-rigid conformation of $\mathbf{1}^{\bullet-}$ in solution with a variation of the dihedral angle of the two indole rings. In fact, such an undulation of the baseline was not observed in the case of the 4-methyl derivative $\mathbf{4}^{\bullet-}$.

(35) Kenney, W. C.; McIntire, W. *Biochemistry* **1983**, *22*, 3858−3868.
(36) Husain, M.; Davidson, V. L. *Biochemistry* **1987**, *26*, 4139−4143.

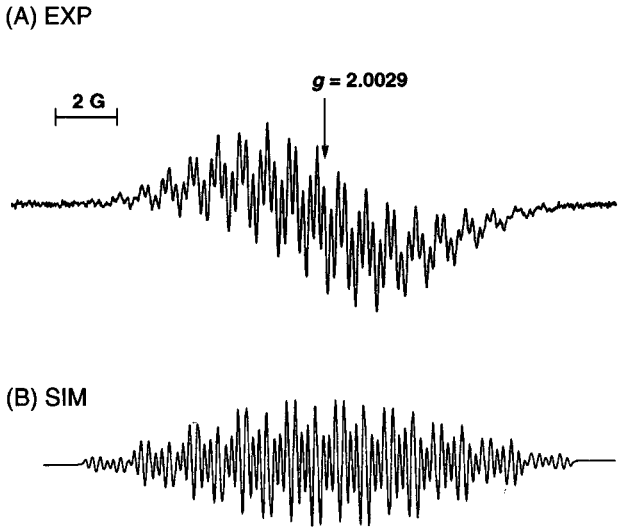

Figure 12. (A) ESR spectrum of the $\mathbf{1}^{\bullet-}-Mg^{2+}$ complex generated by the addition of $Mg(ClO_4)_2$ (5.0×10^{-4} M) into CH_3OH solution of half-reduced **1** (5.0×10^{-4} M) with $NaBH_4$ under anaerobic condition. (B) Computer simulation spectrum of $\mathbf{1}^{\bullet-}-Mg^{2+}$; $\Delta H_1 = 0.05$ G.

in Chart 2. It is clearly shown that the spin densities on the indole ring at the 4-position in $Mg^{2+}-\mathbf{1}^{\bullet-}$ are significantly decreased by the coordination to Mg^{2+}.

Summary and Conclusions

The extensive data for the visible−NIR spectra and the binding constants for a series of metal ion complexes of the TTQ model compounds reported in this study provide useful clues to identify the cationic species involved in TTQ-dependent enzymes.[37] In particular, intramolecular charge transfer bands from the indole ring to the quinone moiety of metal ion complexes are highly sensitive to the type of metal ions and the charge-transfer energies are well correlated with the binding strength of the metal ions to TTQ model compounds (Figure 3). In the presence of the amine substrate, deportation of the pyrrole proton 1-NH takes place to enhance the binding with monovalent and divalent metal ions, whereas the binding strength of trivalent metal ions is reduced in the presence of the amine.

The enhancement of the oxidizing ability of TTQ model compounds is shown by large positive shifts in the one-electron reduction potentials of metal ion complexes of the TTQ model compound as compared to those in the absence of the metal ion. This indicates the much stronger binding of the radical anions of TTQ model compounds with metal ions as compared to the neutral compounds. The interaction between the radical anion and the Mg^{2+} ion is directly detected by the ESR spectrum in comparison with that of the radical anion without metal ion. The delocalization of spin into the indole aromatic rings in $\mathbf{1}^{\bullet-}$ implies an important role of indole as an electron-transfer route from the reduced TTQ to the copper site of electron-acceptor enzymes.

The metal ion complex of TTQ model compound is shown to oxidize not only benzylamine but also aliphatic amines in anhydrous organic media whereas no reaction takes place in the absence of the metal ion under otherwise the same experimental conditions. Metal ions are shown to accelerate each step in three distinct steps: the addition of the amine to the quinone, the spontaneous and the amine-catalyzed rearrangement from the substrate imine to the product imine, and the imine exchange reaction to generate the aminophenol and $RCH_2N{=}CHR$ (Scheme 2). Thus, cationic species involved in the enzyme may also act as a catalyst to promote the amine-oxidation reaction.

Acknowledgment. The present study was financially supported in part by a Grant-in-Aid for Scientific Research from the Ministry of Education, Science, Culture, and Sports of Japan.

JA0020207

(37) However, more data on the TTQ-dependent enzymatic systems are required to specify the cationic species involved in the enzymatic systems in comparison with the model systems.